JOURNAL OF SPACECRAFT AND ROCKETS
Vol. 38, No. 2, March–April 2001

Satellite Formation Flying Design and Evolution

Chris Sabol,* Rich Burns,† and Craig A. McLaughlin‡
U.S. Air Force Research Laboratory, Kirtland Air Force Base, New Mexico 87117-5776

Several satellite formation flying designs and their evolution through time are investigated. Satellite formation flying designs are derived from the linearized equations of relative motion under two-body dynamics better known as Hill's equations (Hill, G. W., "Researches in the Lunar Theory," *American Journal of Mathematics*, Vol. 1, No. 1, 1878, pp. 5–26). The formations are then propagated forward in time in the presence of realistic perturbations to determine the stability of each design. Formations considered include in-plane, in-track, circular, and projected circular designs. The Draper Semianalytic Satellite Theory is used to propagate mean elements of the satellites. When perturbations disrupt the satellite formations, an effort is made to quantify the cost of formation-keeping maneuvers. The goal of this effort is to provide physical insight into satellite formation flying design and outline the effects of realistic dynamics on those designs.

Nomenclature

a	=	semimajor axis, km
$\boldsymbol{a}_{dh}$	=	acceleration in the direction of angular momentum vector, m/s^2
a_{dn}	=	acceleration in the normal direction, m/s^2
$\boldsymbol{a}_{dt}$	=	acceleration in the direction of velocity vector, m/s^2
e	=	eccentricity
f	=	true anomaly, deg
h	=	angular momentum, m^2/s
i	=	inclination, deg
J_2	=	geopotential coefficient representing Earth's oblateness
M	=	mean anomaly, deg
n	=	mean motion, 1/s
p	=	semilatus rectum, km
r	=	radius of circular or projected circular formation (cluster radius), km
t	=	time, s
v	=	magnitude of velocity, km/s
x	=	radial difference between two objects in Hill's equations,[8] km
y	=	along-track difference between two objects in Hill's equations,[8] km
z	=	cross-track difference between two objects in Hill's equations,[8] km
Δa	=	change in semimajor axis, km
ΔM	=	mean anomaly separation, rad
Δt	=	time interval, s
Δv	=	change in velocity, m/s
$\Delta\Omega$	=	nodal separation, deg
δi	=	inclination difference in formation, deg
$\delta\dot{\Omega}$	=	difference between nodal regression rates, rad/s
θ	=	phase angle of satellite for circular or projected circular formations, deg measured counterclockwise from cross-track (z) direction in the plane of relative motion, deg
μ	=	Earth's gravitational constant, km^3/s^2
Ω	=	right ascension of the ascending node, deg
ω	=	argument of perigee, deg
ω_e	=	rotation rate of Earth, deg/s

Subscript

0	=	initial value

Introduction

IN recent years, there has been increasing interest in the use of satellites flying in formation. Several missions and mission statements have identified formation flying as a means of reducing cost and adding flexibility to space-based programs. Mission planners hope to reduce size and complexity of single large spacecraft missions in favor of flying several smaller, less complicated satellites. Flying multiple satellites in formation offers flexibility to mission designers because the individual satellites can reposition themselves with respect to each other to perform different tasks. For instance, a ground observing space-based sensor may choose to fly a formation of satellites to increase aperture size rather than trying to construct a very large satellite. The system adds flexibility because the formation and, therefore, aperture size and orientation are adjustable on orbit.

Formation flying clusters of satellites also provide for graceful degradation of performance during times of satellite failure. If a single large satellite has a system failure, the entire mission is at risk. If a single satellite in a cluster fails, the remaining satellites in the cluster may continue to perform the mission at a lower performance level. The cluster could then be brought back up to mission design specifications with the addition of another inexpensive replacement satellite or improved with the addition of an upgraded satellite.

Several missions are using or considering satellite formations to accomplish goals that are not possible or are very difficult to accomplish with a single satellite. NASA's New Millennium program has identified the benefits of satellite formation flying and has included an enhanced formation flying experiment in the Earth Observing-1 mission.[1,2] The ESA has developed an elaborate formation for its Cluster mission to study the Earth's magnetosphere.[3] The Orion program is meant to be a low-cost demonstration of global positioning system uses in formation flying.[4] The Laser Interferometer Space Antenna (LISA) mission is a heliocentric formation flying mission designed to detect gravity waves.[5] The U.S. Air Force Research Laboratory's TechSat 21 program is a technology demonstration of the virtual satellite concept.[6,7] It is likely that there are other missions considering formation flying.

In this study, the relative equations of motion of two satellites, known as Hill's equations,[8] are used. Sedwick et al.[9] present Hill's equations[8] for use in formation flying and provide a simple analysis of J_2, drag, solar radiation pressure, and electromagnetic perturbations. This study gives a more detailed examination of formation design and the effects of perturbations. From the solutions to Hill's equations,[8] several satellite formation flying designs are described. Next, test cases for each of the formation designs are propagated in the presence of realistic perturbations. The Draper Semianalytic

Presented as Paper 99-121 at the AAS/AIAA Spaceflight Mechanics Meeting, Breckenridge, CO, 7 February 1999; received 24 February 2000; revision received 20 December 2000; accepted for publication 3 January 2001.

*Research Engineer, Directed Energy Directorate.
†Research Engineer, Space Vehicles Directorate. Member AIAA.
‡Research Aerospace Engineer, Space Vehicles Directorate. Senior Member AIAA.

Satellite Theory (DSST) is used to propagate the averaged equations of motion in the presence of a gravity field of degree and order 21, luni–solar third-body point-mass effects, atmospheric drag, and solar radiation pressure. By the comparison of the trajectories, an effort is made to identify the perturbations that disrupt the formations and to provide insight into the maneuvers required for correcting these effects.

An overview of the effects of differential orbital elements on formation behavior will help provide insight into formation design. Orbits with different semimajor axes will have different periods. Different periods cause the formation to disperse rapidly. Therefore, it is required that the mean semimajor axis be the same for all satellites in a formation. Differences in inclination cause the formation to have out-of-plane separation at higher latitudes, but not at the equator. Inclination differences also cause the satellites to have different nodal precession rates caused by J_2. The differences in nodal precession rates cause the orbital planes to separate and the formation separation to grow. Satellites with differences in the right ascension of the ascending node will have maximum separation over the equator and less at higher latitudes. If the orbits are in the same plane, differences in mean anomaly will give along-track separation. Finally, for orbits with some eccentricity, differences in argument of perigee will give relative motion in the radial direction.

Formation Designs

Satellite formation flying designs can be derived from the linearized equations of relative motion for two objects under the influence of a point-mass gravitational field. These equations are commonly known as Hill's equations.[8] Vallado[10] provides a detailed derivation of Hill's equations[8] that take the following form for unperturbed motion:

$$\ddot{x} - 2n\dot{y} - 3n^2x = 0 \tag{1}$$

$$\ddot{y} + 2n\dot{x} = 0 \tag{2}$$

$$\ddot{z} + n^2z = 0 \tag{3}$$

where the mean motion is that of the reference object.

Two major assumptions are inherent in Hill's equations[8]: 1) the reference object is in a circular orbit and 2) the distance between the objects is small in comparison to their orbital radii to support simplifications. Lawden[11] was the first to develop equations of relative motion including eccentricity. Later developments for eccentric orbits are summarized by Inalhan and How.[12] Spencer[13] includes first-order eccentricity effects of the reference orbit in the equations of relative motion.

Note that Hill's equations[8] have traditionally been used for rendezvous analysis, which is usually concerned with relatively short time spans. The mission planning arena, however, concerns the entire mission lifetime, but it is not clear that the simplifications made in the derivation of Hill's equations will remain valid over such an extended time period. Hence, Hill's equations are used as a preliminary design tool, complemented with numerical simulation of the fully nonlinear dynamics with realistic force modeling. Future designs may benefit from a careful analysis of the fully nonlinear equations of relative motion.

The unperturbed version of Hill's equations[8] can be solved analytically. The solution is

$$x(t) = (\dot{x}_0/n)\sin nt - (3x_0 + 2\dot{y}_0/n)\cos nt + 4x_0 + 2\dot{y}_0/n \tag{4}$$

$$y(t) = (2\dot{x}_0/n)\cos nt + (6x_0 + 4\dot{y}_0/n)\sin nt - (6nx_0 + 3\dot{y}_0)t - 2\dot{x}_0/n + y_0 \tag{5}$$

$$z(t) = (\dot{z}_0/n)\sin nt + z_0\cos nt \tag{6}$$

Note the secular term in the second equation. To avoid secular growth in the relative motion, we set the secular term to zero through the constraint

$$\dot{y}_0 = -2x_0n \tag{7}$$

Through algebraic manipulations, it can be shown that this constraint results in a displaced orbit with the same energy, and thus the same semimajor axis, as the reference orbit neglecting higher-order terms in eccentricity. When the constraint is enforced, Hill's equations become

$$x(t) = (\dot{x}_0/n)\sin nt + x_0\cos nt \tag{8}$$

$$y(t) = (2\dot{x}_0/n)\cos nt - 2x_0\sin nt - 2\dot{x}_0/n + y_0 \tag{9}$$

$$z(t) = (\dot{z}_0/n)\sin nt + z_0\cos nt \tag{10}$$

These equations provide the basis for formation flying design.

In the preceding equations, it can be seen that the radial, x, and along-track, y, components of motion are uncoupled from the cross-track, z, component of the relative motion. Note that in the nonlinear equations, the out-of-plane motion z is weakly coupled with the radial/along-track plane motion. Vallado[10] shows that the radial/along-track motion can be described by

$$x^2/C^2 + y^2/4C^2 = 1 \tag{11}$$

where

$$C = \sqrt{x_0^2 + (\dot{x}_0/n)^2} \tag{12}$$

when the $\dot{y}_0$ constraint is applied. This equation is an ellipse of fixed eccentricity ($e = \sqrt{3}/2 = 0.866$) with an arbitrary along-track offset. Thus, the motion in the radial/along-track plane will always be an ellipse with the major axis in the along-track direction that is twice the minor axis in the radial direction. All unperturbed formation flying designs must project this elliptical motion into the radial/along-track plane.

In the linearized model, the cross-track, z, component of the relative motion is a simple harmonic oscillator. Combining the elliptical motion in the radial/along-track direction with the oscillatory motion in the cross-track direction yields a family of ellipses that describe all formation flying designs using two-body dynamics.

Six initial conditions must be specified in the solutions to Hill's equations.[8] These initial conditions can be thought of as Cartesian or Keplerian element differences between the two satellites and allow for six constraints or design parameters to be placed on the formation. One constraint was specified when the secular terms were removed from the solutions to Hill's equations. This constraint can be thought of as requiring the semimajor axis of the two satellites to be equal. Another constraint, y_0, is the offset of the elliptical motion in the radial/along-track plane. Now, four design parameters are left that describe the size, eccentricity, orientation, and initial location in the ellipse of relative motion. These constraints can also be thought of as the size of the ellipse in the radial/along-track plane, the initial location within that ellipse, the amplitude of the oscillation in the cross-track plane, and the initial location in the cross-track oscillation.

In this analysis, four formation flying designs are considered. They are in-plane, in-track, circular, and projected circular. Each of these formations is described as follows.

In-Plane Formation

The in-plane formation is the simplest of all cluster designs. The formation consists of a group of satellites occupying the same orbital plane and separated by mean anomaly. In Hill's equations,[8] this formation is represented by setting all initial conditions, except for y_0, to zero. The solutions to Hill's equations are then

$$x(t) = 0 \tag{13}$$

$$y(t) = y_0 \tag{14}$$

$$z(t) = 0 \tag{15}$$

where y_0 represents the amount of in-plane spacing between two satellites. This can be related to the mean anomaly separation by

$$\Delta M = y_0/a \tag{16}$$

Again, this formulation based on Hill's equations assumes that the orbits are circular. The primary advantage of the in-plane formation is its simplicity in design, deployment, and control.

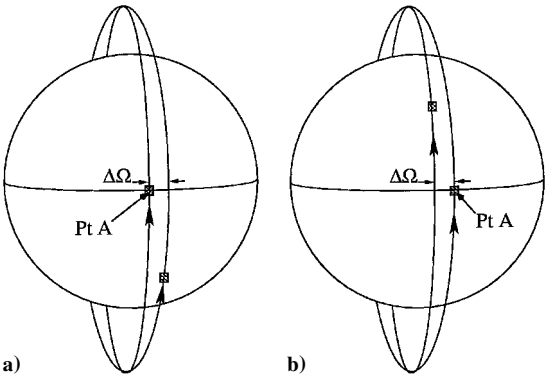

Fig. 1 In-track formation.

In-Track Formation

The in-track cluster design is a slight variation on the in-plane formation. Here the satellites all share the same ground track. Vallado[10] gives more details on ground tracks. To share the same ground track, the satellites have to occupy slightly different orbital planes separated by right ascension of the ascending node, which accounts for the rotation of the Earth.

In Hill's equations,[8] this formation is very similar to the in-plane formation except that a cross-track oscillation represents the difference in right ascension of the ascending node. The solutions to Hill's equations are then

$$x(t) = 0 \tag{17}$$

$$y(t) = y_0 \tag{18}$$

$$z(t) = -(\omega_e/n)y_0 \sin i \cos nt \tag{19}$$

To find the relationship between y_0 and z_0, consider the reference satellite at the ascending node over some point (call it point A) on the Earth's equator. In Fig. 1a, the lead satellite is over point A at time t, The trailing satellite is behind the lead by some difference in mean anomaly; relate this difference in mean anomaly to a difference in time. Then calculate the nodal difference $\Delta\Omega$ such that the second satellite is over point A at time $(t + \Delta t)$ as in Fig. 1b. The equations take the following form:

$$\Delta M = y_0/a \tag{20}$$

$$\Delta t = -(\Delta M/n) = -(y_0/an) \tag{21}$$

$$\Delta\Omega = \omega_e \Delta t = -(\omega_e y_0/an) = z_0/a \sin i \tag{22}$$

$$z_0 = -(\omega_e/n)y_0 \sin i \tag{23}$$

Again, this formulation based on Hill's equations assumes that the orbits are circular and the satellites are close. The attractiveness of the in-track formation is that each satellite in the formation passes over the same exact spots on the ground, which is valuable for Earth sensing missions.

Circular Formation

As the name implies, the circular formation is one in which satellites maintain a constant distance from each other. The formation can be derived from Hill's equations[8] analytically or geometrically. The analytic approach takes the solutions to Hill's equations and determines relations between the initial conditions given the constraint

$$x^2 + y^2 + z^2 = r^2 \tag{24}$$

where r is the radius of the formation. The geometric approach takes advantage of the fact that the relative motion in the radial/along-track planes (x/y) is fixed in eccentricity. From either approach, the following relations are found by substituting the constraints into Hill's equations:

$$\dot{y}_0 = -2nx_0 \tag{25}$$

$$y_0 = 2\dot{x}_0/n \tag{26}$$

$$z_0 = \pm\sqrt{3}x_0 \tag{27}$$

$$\dot{z}_0 = \pm\sqrt{3}\dot{x}_0 \tag{28}$$

where the first two conditions (25) and (26) set the along-track drift and offset to zero. The sign in Eqs. (27) and (28) must be the same for a given case. These constraints show that there are two planes in which the circular formation is possible. Both planes intersect the cross-track/along-track plane along the along-track axis but one is inclined 30 deg to that plane and the other is inclined at −30 deg.

If the 30-deg case is chosen, the following solutions to Hill's equations[8] are found:

$$x(t) = (\dot{x}_0/n) \sin nt + x_0 \cos nt \tag{29}$$

$$y(t) = (2\dot{x}_0/n) \cos nt - 2x_0 \sin nt \tag{30}$$

$$z(t) = \sqrt{3}(\dot{x}_0/n) \sin nt + \sqrt{3}x_0 \cos nt \tag{31}$$

Note that the formation design has two free parameters: x_0 and $\dot{x}_0$. These free parameters specify the radius and phasing of one satellite in its circular path about the reference satellite. The four other initial conditions were constrained for eliminating along-track drift, eliminating the along-track offset, and setting the eccentricity and orientation of the ellipse of relative motion.

If the initial conditions of the solutions to Hill's equations[8] presented in Eqs. (25–28) are formulated in terms of the cluster radius and phasing, the following equations arise:

$$x_0 = (r/2) \cos\theta \tag{32}$$

$$\dot{x}_0 = -(rn/2) \sin\theta \tag{33}$$

From Eqs. (29–33), given a circular reference orbit and desired cluster radius and phasing, one could convert the reference elements from Keplerian to Cartesian, after coordinate transformations add the Cartesian differences to get the position and velocity vectors of the satellites in the circular cluster, and then convert the Cartesian elements back to Keplerian for all satellites in the cluster. This formation design approach was taken here. Note that the conversion from Cartesian to Keplerian will expose small errors in the semimajor axis on the order of e. The semimajor axes of the satellites are corrected to the same value so the two-body periods match.

The Keplerian element differences for a circular formation are highly dependent on the phasing and initial conditions of the reference orbit. For two arbitrary points in the cluster, there will be differences in inclination, right ascension of the ascending node, argument of perigee, and mean anomaly. Generally, satellites in the cluster will have the same eccentricity except the case where the reference orbit is not circular. There are conditions, however, where two satellites in the cluster can have the same inclination or right ascension of the ascending node.

To provide physical insight into the circular formation design in terms of Keplerian mechanics, consider a circular reference orbit inclined at 90 deg with a satellite at the equator (ascending node). Consider another satellite in a slightly elliptical orbit also on the equator and separated from the reference orbit by a small amount of ascending node. The second satellite is at apogee and, therefore, will fall behind the reference satellite as they both proceed toward the north pole. Because both orbits are polar, the satellite's paths will cross at the poles, but the reference satellite reaches the pole first. On the other side of the north pole, the second satellite is lower in altitude than the reference satellite and begins to catch up. Both satellites reach their descending nodes at the same time, and the second satellite is now at perigee. The second satellite continues to advance ahead of the reference satellite and reaches the south pole first, where the paths cross once again. On the other side of the south pole, the reference satellite begins to catch up as the second satellite increases in altitude toward its apogee at the ascending node.

The circular formation has two properties that make it attractive: 1) the satellites maintain a constant distance from each other and

2) unlike the in-plane and in-track formations, the circular cluster presents a two-dimensional array.

Projected Circular Formation

The projected circular formation is very close in design to the circular formation. The difference is that the projected circular cluster only maintains a fixed distance in the along-track/cross-track (y/z) plane. Another way to describe the projected circular formation is to say that when the ellipse of relative motion is projected on to the along-track/cross-track plane, it produces a circle. The constraint

$$y^2 + z^2 = r^2 \tag{34}$$

is the result.

Like the circular cluster, the constraint can be applied to the initial conditions to the solutions of Hill's equations[8] to produce

$$\dot{y}_0 = -2nx_0 \tag{35}$$

$$y_0 = 2\dot{x}_0/n \tag{36}$$

$$z_0 = \pm 2x_0 \tag{37}$$

$$\dot{z}_0 = \pm 2\dot{x}_0 \tag{38}$$

where the first two conditions set the along-track drift and offset to zero. The signs on Eqs. (37) and (38) must be the same. There are two planes in which the projected circular formation is possible. Both intersect the cross-track/along-track plane along the along-track axis, but one is inclined 26.565 deg to that plane and the other is inclined at −26.565 deg.

If the 26.565-deg case is chosen, the following solutions to Hill's equations[8] are found:

$$x(t) = (\dot{x}_0/n)\sin nt + x_0 \cos nt \tag{39}$$

$$y(t) = (2\dot{x}_0/n)\cos nt - 2x_0 \sin nt \tag{40}$$

$$z(t) = (2\dot{x}_0/n)\sin nt + 2x_0 \cos nt \tag{41}$$

The formation design has two free parameters that represent the radius and phasing of projected circular path.

If the initial conditions of the solutions to Hill's equations[8] presented in Eqs. (35–38) are formulated in terms of the cluster radius and phasing, the following arises:

$$x_0 = (r/2)\cos\theta \tag{42}$$

$$\dot{x}_0 = -(rn/2)\sin\theta \tag{43}$$

Like the circular formation design, the Keplerian element differences appear in inclination, right ascension of the ascending node, argument of perigee, and mean anomaly. The variations are dependent on the reference orbit and the phasing.

The primary advantage of the projected circular cluster over the circular cluster is that the satellites are separated by a fixed distance when the formation is projected onto the along-track/cross-track plane. This characteristic has applications for ground observing missions.

Propagations

Test cases of the formation designs were propagated for 1 year in the presence of realistic dynamics. The DSST Averaged Orbit Generator (AOG) was used to propagate mean elements for each of the test cases. DSST was chosen for its rigorous modeling of the averaged equations of motion. This allows for fast, efficient, and accurate orbit propagation over long periods using step sizes on the order of 1 day. McClain,[14] Danielson,[15] Feiger,[16] Sabol et al.,[17] and Fonte[18] provide more information on the formulation and accuracy of the DSST. The DSST runs were executed with the Draper Research and Development version of the Goddard Trajectory Determination System (DGTDS).[18]

The perturbations modeled in the propagations include a geopotential to degree and order 21, atmospheric drag effects, luni–solar third-body point-mass effects, and solar radiation pressure. Table 1 lists the specifics of the ephemeris generations.

The Jacchia–Roberts atmospheric density model is dependent on daily F10.7 cm solar flux and 3 hourly values of the k_p geomagnetic indices. Schatten et al.[19] and Sofia and Schatten[20] developed a method to predict smoothed estimates of these parameters over the solar cycle. The solar flux and geomagnetic indices used in this analysis are the hot or maximum value predictions from 1994. It was felt that the hot atmosphere prediction would provide a conservative estimate of drag effects. Identical area-to-mass ratios of 0.01 m^2/kg were used for each spacecraft in drag and solar radiation pressure calculations.

For each of the formation flying designs, two orbits were propagated: one representing the reference satellite and the second representing another satellite in the formation. The trajectories were then compared over the year-long arc to determine the stability of the formations in the presence of perturbations.

Note that the elements resulting from the formation designs and input into the DGTDS DSST propagator are assumed to be averaged elements. If the two-body-based Keplerian elements are assumed to be osculating in the presence of perturbations, the mean semimajor axes will not match, and the formation design specifications will not hold.

Results

In this section, the results of the formation flying designs and propagations are presented. All cases are polar, near 800 km in altitude with a satellite spacing of approximately 1 km. All satellites in a given formation have the same mean semimajor axis. Satellite 1 always has $e = 10^{-6}$, $i = 90$ deg, and $\omega = M = 0$. Satellite 1 has $\Omega = 0$ for all except the in-plane formation. For the in-plane formation, $\Omega = 10$ deg to avoid coupling effects that may be an artifact of the integration process and not real effects. Table 2 gives the elements for satellite 2 in the in-plane and in-track formations. The elements for the other satellites in the circular formation are given in Table 3.

Table 1 DSST propagation description

Characteristic	Setting
Start time	15 Sept. 1998, 0 h, 0 min, 0 s
End time	15 Sept. 1999, 0 h, 0 min, 0 s
Integrator	12th-order summed Cowell/Adams predict partial correct
Step size	12 h
Geopotential	21 × 21 JGM2
Atmospheric drag	Jacchia–Roberts, $C_D = 2.0$ Hot Schatten solar flux, k_p prediction
Third body	Solar/lunar point masses based on Jet Propulsion Laboratory ephemerides
Solar radiation pressure	Cylindrical shadow model, $C_r = 1.2$

Table 2 Initial mean orbital elements of satellite 2 for in-plane and in-track formations

Orbital element	In plane, 100:7	In plane, 14:1	In track, 100:7	In track, 14:1
a, km	7155.422	7252.636	7155.422	7252.636
e	10^{-6}	10^{-6}	10^{-6}	10^{-6}
i, deg	90	90	90	90
Ω, deg	10	10	0.00057	0.00057
ω, deg	0	0	0	0
M, deg	0.008007	0.008007	−0.008007	−0.008007

Table 3 Initial mean orbital elements for the circular formation

Orbital element	Satellite 2	Satellite 3
a, km	7178.1363 km	7178.1363 km
e	6.965597×10^{-5}	6.965463×10^{-5}
i, deg	90.0069126	90
Ω, deg	0.00000121	0.00691308
ω, deg	270.0248415	0
M, deg	89.9751584	0

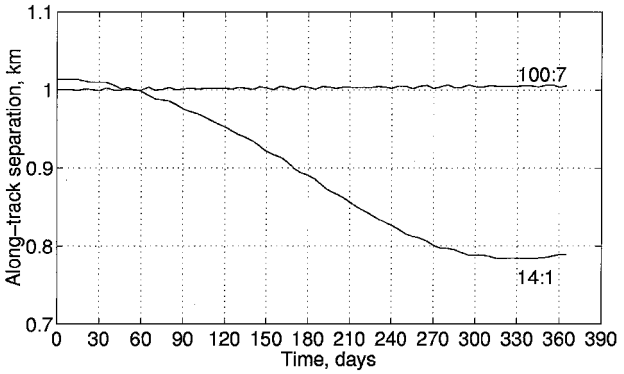

Fig. 2 Along-track separation for the in-plane formation.

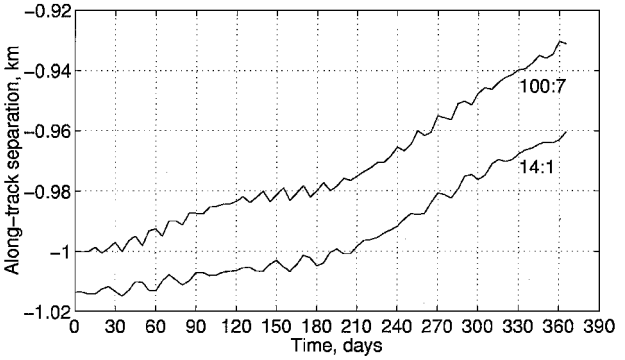

Fig. 3 Along-track separation for the in-track formation.

In-Plane Formation

Two cases were considered for the in-plane formation. The first corresponded to a 100-revolution-per-seven-nodal-day repeat ground-track cycle, and the second incorporated a 14 revolution per nodal day repeat ground track cycle. Consult Vallado[10] for information on ground tracks and tesseral resonance. Table 2 presents the averaged DSST Keplerian elements for the 100:7 and 14:1 in-plane formation designs.

The year-long ephemeris comparison results for the shallow (100:7) repeat ground-track case showed the in-plane formation to be relatively stable in the presence of perturbations. The difference from the nominal separation was on the order of meters, which is negligible for most applications. This is shown in Fig. 2.

For the daily repeat ground track (14:1) case, tesseral resonance had a much greater effect. The deep tesseral resonance of the 14:1 case pushed the two satellites toward each other. Figure 2 shows the along-track separation for the two satellites. Figure 2 shows the initial 1-km separation gradually drop as tesseral resonance moves the satellites closer together. Figure 2 also shows the drift reverses at around 300 days. Over time, the satellites should oscillate back to their original positions. In terms of Keplerian elements, the tesseral resonance induces very long-period changes in the semimajor axis and mean anomaly (as well as other elements that do not appear to affect the formation greatly); the relative semimajor axis changes are on the centimeter level. Simulations made without the tesserals confirm that the resonance was the cause of the drift.

In-Track Formation

Like the in-plane formation, two cases were considered for the in-track formation. The first corresponded to a 100-revolution-per-seven-nodal-day repeat ground-track cycle and the second incorporated a 14 revolution per nodal day repeat ground-track cycle. Table 2 presents the averaged DSST Keplerian elements for the 100:7 and 14:1 in-track formation designs.

Because the satellites share the same ground track, they encounter the same gravitational effects. The year-long ephemeris comparison for both cases showed no differences due to the effects of tesseral resonance, which is expected due to the nature of the formation design. However, because the satellites are in slightly different orbital planes, atmospheric drag caused a slight along-track drift between the two satellites. This was confirmed by running a case with the drag perturbation turned off. Figure 3 shows the along-track drift between the two satellites for both repeat ground-track cases.

Figure 3 shows the along-track drift for the deep resonance case to be on the order of 50 m by the end of the year. The along-track error growth was closer to 70 m for the lower altitude shallow resonance case. In terms of Keplerian elements, the along-track drift can be traced to a subcentimeter difference in semimajor axis. Note once again that a high-density atmosphere is being used in the drag predictions. Even with the high-density atmosphere, the formation keeping errors could still be considered small over the course of the year.

Circular Formation

Three satellite trajectories were generated for the circular cluster. Satellite 1 represents the center of the circular formation and the reference satellite. Satellite 2 is on the circle with an initial phasing of 270 deg, and satellite 3 is on the circle with an initial phasing of 180 deg. The formation was designed with the initial conditions of the reference satellite at the equator on the ascending node. This design puts satellite 2 directly ahead of satellite 1 in the along-track direction and satellite 3 to the right of satellite 1 in the negative cross-track direction at epoch. Table 3 presents the averaged DSST Keplerian elements for the circular formation design. These elements were chosen to place the cluster at an altitude of 800 km.

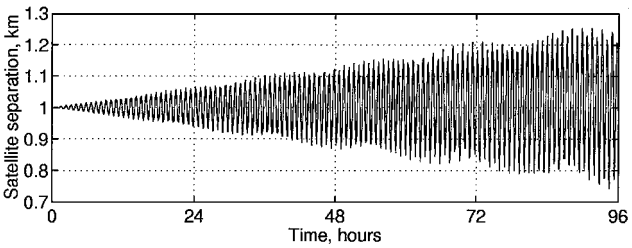

Fig. 4a Separation between satellite 1 and satellite 2.

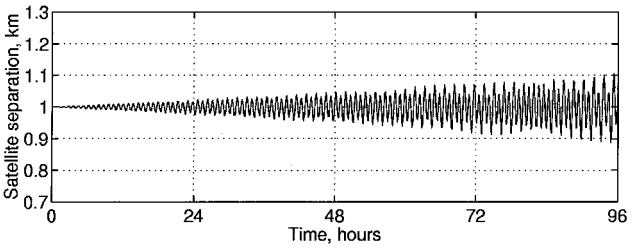

Fig. 4b Separation between satellite 1 and satellite 3.

Propagations in the presence of perturbations show the circular formation to be unstable. The primary factor disrupting the formation design is the Earth's oblateness or J_2 effect. The J_2 contributions to the relative motion are at least an order of magnitude larger than the other disturbing accelerations including tesseral resonance (for short repeat ground-track cases), atmospheric drag, solar radiation pressure, and third-body gravitational effects. Earth oblateness effects are most prevalent in the secular motion of the right ascension of the ascending node, argument of perigee, and mean anomaly.

Figure 4a shows the position separation between satellites 1 and 2 over four days. Figure 4a shows the separation varies by about ± 250 m from the nominal of 1 km. This error growth is mostly in the cross-track direction. Examination of the Keplerian element histories revealed that this cross-track error growth can be attributed to the difference in precession rates of the right ascension of the ascending node. Because the two orbital planes have slightly different inclinations, the secular J_2 effect causes the right ascension of the ascending node for each orbit to precess at slightly different rates. Differential nodal precession results in the orbital planes drifting apart and a cross-track error growth. The following nodal

regression analysis is similar to that by Alfriend et al.[21] Assuming the growth is in the cross-track direction, the equations are

$$x = \tfrac{1}{2}\sin nt \tag{44}$$

$$y = \cos nt \tag{45}$$

$$z = \left(\sqrt{3}/2\right)\sin nt - a\delta\dot{\Omega}t\cos nt \tag{46}$$

Solving for the radius of the formation gives

$$r = \sqrt{1 - \sqrt{3}a\delta\dot{\Omega}t\sin nt\cos nt + (a\delta\dot{\Omega}t)^2\cos^2 nt} \tag{47}$$

where $\delta\dot{\Omega}$ is the differential nodal regression rate between the satellites. Over four days, the maximum growth in the separation using these equations is 195 m compared to 256 m from DSST using higher-order perturbations.

An additional contribution to the error growth is caused by the rotation of the line of apsides of the orbits. For the polar orbit configuration, the J_2 effect is nearly equal and opposite on the mean anomaly and the argument of perigee. This effect makes little difference for the circular orbit of satellite 1, but for satellite 2 the orbit line of apsides begins to rotate and disrupt the formation design. For this configuration, the line of apsides is rotated greater than 3 deg per day by the J_2 effect. The effect can not be discerned by simply noting the differential rotation angle. Instead, the total separation growth is caused by a phase change in the x, y, and z components. The reason for this is that the radial/along-track motion is phased relative to the perigee, but the cross-track motion is phased relative to the nodal crossing. For a polar orbit, J_2 causes the mean anomaly to increase faster than the two-body mean motion. The phasing in the radial/along-track plane is, therefore, changed. In the cross-track plane, the phasing is relative to the node and so it is affected by J_2 effects on both argument of perigee and mean anomaly. Taking Eqs. (44–46) and adding these effects gives

$$x = \tfrac{1}{2}\sin(nt - \dot{M}t) \tag{48}$$

$$y = \cos(nt - \dot{M}t) \tag{49}$$

$$z = \left(\sqrt{3}/2\right)\sin(nt - \dot{M}t + \dot{\omega}t) - a\delta\dot{\Omega}t\cos(nt - \dot{M}t + \dot{\omega}t) \tag{50}$$

where $\dot{M}$ and $\dot{\omega}$ are the secular mean anomaly rate and the secular argument of perigee rate of satellite 1 caused by J_2. These equations give a maximum growth in separation of 246 m after four days. Compare this with 256 m from DSST using higher-order perturbations. In addition, these equations accurately track the motion in each component.

Figure 4b shows the position separation between satellites 1 and 3 over four days. Here, the separation varies from the nominal 1 km by about ±110 m. Again, the dominant disturbing force is Earth oblateness, and the error growth is caused by the rotation of the line of apsides for the orbits. Because satellites 1 and 3 share the same inclination, the large cross-track error growth is not present. In fact, there is no discernible growth in the radial, cross-track, or along-track separation. The growth in the total separation is caused by phasing differences in the three components as discussed earlier. Here the equations to describe the motion are

$$x = -\tfrac{1}{2}\cos(nt - \dot{M}t) \tag{51}$$

$$y = \sin(nt - \dot{M}t) \tag{52}$$

$$z = -\left(\sqrt{3}/2\right)\cos(nt - \dot{M}t + \dot{\omega}t) \tag{53}$$

These equations give a maximum growth in separation of 86 m after four days compared to 113 m from DSST. The motion of each component is also accurately reproduced by these equations. A further observation is that the $\dot{\omega}$ term will be zero at the critical inclination and all of the components will be in phase. Therefore, there will be much less growth in the total separation at critical inclination.

In addition to the Earth oblateness effects, atmospheric drag, solar radiation pressure, and tesseral resonance (for short repeat ground-track cycles) disrupt the circular formation in much the same way as they disrupt the in-plane and in-track formations. In fact, the effects of these perturbations are greater on the circular formation because the differences in the satellite orbital planes are larger for the circular formation design than the two earlier cases.

Projected Circular Formation

No additional propagations were performed to analyze the effects of perturbations on the projected circular formation. Instead, the insight and understanding presented in the circular formation analysis is referenced.

Because the projected circular formation shares many of the same design characteristics as the circular formation in terms of Keplerian element differences between the reference satellite and other satellites in the formations, the effects of perturbations on the projected circular formation will be the same as the effects on the circular formation. The projected circular design requires similar levels of eccentricity, inclination, right ascension of the ascending node, argument of perigee, and mean anomaly differences as the circular formation designs. Thus, the J_2 effects that are dominant in the disruption of the circular formation are equally disruptive to the projected circular formation.

Formation and Station Keeping

The results of the propagations indicated that maneuvers are necessary to maintain a satellite formation flying design in the presence of perturbations. In this section, the results of the orbit propagations are put into the context of formation and station keeping. An attempt is made to quantify the total formation and station keeping maneuver requirements for the test cases.

Formation Keeping

Perturbations affect the formation designs differently. The in-plane design appeared to be relatively stable in the presence of perturbations with the exception of deep tesseral resonance for short repeat ground-track cycle orbits. The in-track design faced only small atmospheric drag effects. The circular and projected circular formations were unstable. The circular formation separation grew by 25% over four days. Therefore, formation keeping maneuvers are required to account for Earth oblateness, atmospheric drag, and tesseral resonance (for short repeat ground-track cycle orbits) effects.

Both atmospheric drag and tesseral resonance affect the formations in the along-track direction. The along-track error growth induced by these perturbations can be controlled via small adjustments in the semimajor axis of the satellites. Based on the results of the propagations, these semimajor axis adjustments are subcentimeter for drag effects and on the centimeter level for deep tesseral resonance. From Gauss's variation of parameters equations for Keplerian elements in the normal-tangential plane, the change in semimajor axis due to a disturbing acceleration is[22]

$$\dot{a} = (2a^2 v/\mu)\boldsymbol{a}_{dt} \tag{54}$$

If a velocity impulse is assumed, Eq. (54) can be rearranged to determine the velocity impulse required to produce a desired change in semimajor axis:

$$\Delta v_t = (\mu/2a^2 v)\Delta a \tag{55}$$

where the changes in velocity Δv and semimajor axis Δa are assumed small compared to the nominal values. From Eq. (55), it can be shown that, to change the semimajor axis by 1 cm, a velocity impulse of 0.00052 cm/s is required for an 800-km altitude near-circular orbit. Thus, the Δv, and, therefore, propellant requirements, to account for the differential drag and tesseral resonance effects will be quite small. The frequency of the maneuvers will depend on the extent of the drag and resonance effects, formation keeping error bounds, and several control related issues, such as the accuracy with which these maneuvers are performed.

The effects of J_2 were seen in the cross-track direction with indirect along-track contributions. In terms of Keplerian elements, the J_2 secular effects on right ascension of the ascending node, argument of perigee, and mean anomaly are of concern. From Battin,[22]

the change in right ascension of the ascending node due to an out-of-plane (cross-track) acceleration is

$$\dot{\Omega} = \frac{r \sin(\omega + f)}{h \sin i} a_{dh} \tag{56}$$

If a velocity impulse is assumed, Eq. (56) can be rearranged to determine the velocity impulse required to produce a desired change in right ascension of the ascending node:

$$\Delta v_h = \frac{h \sin i}{r \sin(\omega + f)} \Delta\Omega \tag{57}$$

where the changes are assumed small. The differential oblateness effects on right ascension of the ascending node can be derived analytically by taking the partial derivative of the governing equation with respect to the inclination:

$$\dot{\Omega} = -\frac{3}{2} J_2 \left(\frac{R_e}{p}\right)^2 n \cos i \tag{58}$$

$$\delta\dot{\Omega} = \frac{\partial \dot{\Omega}}{\partial i} \delta i = \frac{3}{2} J_2 \left(\frac{R_e}{p}\right)^2 n \sin i \, \delta i \tag{59}$$

where the relationship between Ω and J_2 is taken from Vallado.[10]

When Eqs. (57) and (59) are combined, it is seen that the amount of velocity impulse required to maintain nodal spacing is proportional to the size of the formation and the length of the mission:

$$\Delta\Omega = \delta\dot{\Omega} \Delta t \tag{60}$$

$$\Delta v_h = \frac{h \sin i}{r \sin(\omega + f)} \frac{3}{2} J_2 \left(\frac{R_e}{p}\right)^2 n \sin i \, \delta i \, \Delta t \tag{61}$$

If the near-circular assumption is made, Eq. (61) simplifies to

$$\Delta v_h = \frac{n^2 \sin^2 i}{a \sin(\omega + f)} \frac{3}{2} J_2 R_e^2 \delta i \, \Delta t \tag{62}$$

The total Δv requirement is approximately 38 m/s/km of separation per year for a 800-km altitude polar formation. Note that the maneuvers must be performed at ± 90 deg from nodal crossings to avoid disturbing the inclination.

The second disruptive influence of the Earth's oblateness on satellite formation flying is the rotation of the orbit line of apsides. For polar, near-circular orbits, the effects of J_2 on the argument of perigee and mean anomaly are nearly equal and opposite[10]:

$$\dot{\omega} = \tfrac{3}{4} J_2 (R_e/p)^2 n (4 - 5 \sin^2 i) \tag{63}$$

$$\dot{M}_0 = \tfrac{3}{4} J_2 (R_e/p)^2 \sqrt{1 - e^2}\, n (3 \sin^2 i - 2) \tag{64}$$

The effects of accelerations in the normal direction are also nearly equal and opposite on these elements for near circular orbits[22]:

$$\frac{\mathrm{d}\omega}{\mathrm{d}t} = \frac{1}{ev} \left(2e + \frac{r}{a} \cos f\right) a_{dn} \tag{65}$$

$$\frac{\mathrm{d}M}{\mathrm{d}t} = \frac{-b}{eav} \left(\frac{r}{a} \cos f\right) a_{dn} \tag{66}$$

In Eq. (65), only accelerations in the normal direction (mutually perpendicular to h and v and pointed toward Earth) are considered because impulses in the tangential (velocity) direction would affect semimajor axis and maneuvers in the cross-track direction do not affect the mean anomaly.

Because the effects of these maneuvers are nearly equal and opposite on the mean anomaly and argument of perigee, the formation keeping analysis can be focused on maintaining either one of the elements with maneuvers in the normal direction. This scheme assumes that the other element will be maintained by those maneuvers as well. In this analysis, maintenance of the argument of perigee is studied.

If impulsive maneuvers are assumed, Eq. (65) can be rewritten in terms of the amount of velocity impulse required for a given change in argument of perigee:

$$\Delta v_n = (ev/\cos f) \Delta\omega \tag{67}$$

where the eccentricity is considered to be small. The required change in argument of perigee for a polar orbit can be derived from Eq. (63):

$$\Delta\omega = \dot{\omega} \Delta t = -\tfrac{3}{4} J_2 (R_e/p)^2 n \Delta t \tag{68}$$

$$\Delta v_n = (ev/\cos f) \tfrac{3}{4} J_2 (R_e/p)^2 n \Delta t \tag{69}$$

where the amount of Δv required is again a function of the length of the mission. For an 800-km altitude polar formation, the total Δv requirement is approximately 10.9 m/s per year. Note that the maneuvers must be performed at apogee or perigee to avoid disturbing the eccentricity.

The effects of Earth's oblateness on satellite formation flying designs like the circular and projected circular clusters will require substantial formation keeping maneuvers. There are two components of motion that must be accounted for: 1) differential changes in the right ascension of the ascending node and 2) secular changes in the argument of perigee and mean anomaly. The cost to maintain relative node spacing is dependent on the size of the formation. For a circular cluster of 1 km radius, the cost is approximately 38 m/s per year of velocity impulse. The cost to maintain the argument of perigee is not a function of the cluster size and is roughly 11 m/s per year for the circular cluster. If the maneuvers cannot be coupled, a cluster like the circular formation test case cited earlier could require close to 50 m/s per year of velocity impulse. Based on the orbit propagations and an assumed 10% error bound on the formation, maneuvers would be required every 30 or so hours. Other perturbing effects may also require maneuvers, but at far less frequency and cost than the oblateness-induced maneuvers. Also note that maneuvers may be required in all directions and that each satellite in the formation must be able to thrust in the along-track, cross-track, and radial directions.

The amount of formation keeping maneuvers will also vary from satellite to satellite within the formation. The preceding analysis looked at one of the worst cases. Other satellites within the same formation may require far less formation keeping. This difference in maneuver cost will result in satellites having different masses. Different masses will then map into differential drag and solar radiation pressure errors that must be accounted for. However, the cost of these maneuvers is far less than the cost of the oblateness-induced maneuvers and should not significantly impact the overall cost. The greatest impact is that more frequent along-track maneuvers would be required.

Station Keeping

The primary station keeping concerns for all of the formation flying designs is atmospheric drag. For an 800-km altitude satellite, atmospheric drag could decay the orbit's semimajor axis by close to 3 km in one year. Of course, the effects of drag are dependent on the satellite altitude, area-to-mass ratio, drag coefficient, and the atmospheric density, which is a function of the solar cycle. A high-density atmosphere near the peak of the solar cycle was used in this analysis and so the drag estimates are conservative.

Figure 5 shows the semimajor axis decay for the satellite 1 reference orbit of the circular formation design test case. The decay is almost linear but has some variation due to the orbital orientation to the sun and the time of year. Station keeping a 3-km per year decay in semimajor axis would require approximately 1.5 m/s of velocity impulse. Other perturbations also affect the orbits, but none have substantial secular or long period effects that need to be corrected unless stringent station keeping requirements are made. Table 4 summarizes the formation keeping and station keeping results.

Table 4 Formation keeping and station keeping requirements for circular formation

Maneuver	Δv, m/s/yr
Nodal spacing (formation keeping)	38
Perigee maintenance (formation keeping)	10.9
Drag make-up (station keeping)	1.5
Total	50.4

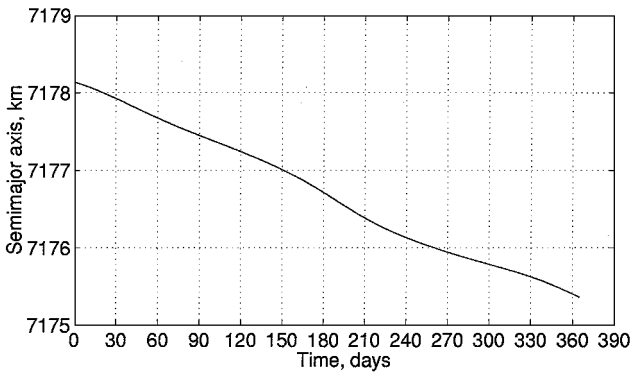

Fig. 5 Semimajor axis decay for an 800-km circular formation.

Conclusions

In this study, four basic satellite formation flying designs were described. Mathematical developments and physical descriptions were given for in-plane, in-track, circular, and projected circular formations. Test cases at roughly 800-km altitude and polar inclination were derived for these formations and were propagated in the presence of realistic dynamics. The propagations showed that perturbations affect each formation differently and can be disruptive to the formation design.

The in-plane formation design appeared to be stable in the presence of perturbations and requires no formation keeping maneuvers. An exception for this case is when the formation design incorporates short-cycle repeat ground-track orbits. Longer repeat ground-track cycles such as the seven day repeat examined here do not significantly affect the formation design. If short-cycle repeat ground tracks are used, deep tesseral resonance requires infrequent, low-cost maneuvers be made in the along-track direction. These maneuvers cost on the order of 0.001 cm/s of velocity impulse per year for a one day repeat cycle.

The in-track formation design is relatively stable but requires small, infrequent, along-track maneuvers to account for atmospheric drag effects. Several factors affect the magnitude of the drag effects, but the maneuver cost will be on the order of 0.0001 cm/s per year for formations spaced closer than 1 km. As the spacing increases, the differential drag effects and, therefore, maneuver cost also increase.

The circular and projected circular formations are unstable due to Earth oblateness effects. Earth oblateness disrupts the formations in two ways: 1) through differential precession of the orbital planes and 2) through rotation of the orbital line of apsides. The differential precession of the orbital planes is a function of inclination differences in the satellite formation. The larger the formation, the larger the inclination differences can be. For the worst-case circular formation, the formation keeping cost is approximately 38 m/s per year per kilometer of formation radius. The rotation of the orbital line of apsides is another major disrupting factor in the circular and projected circular formations. This effect is independent of formation size and should affect all satellites within the formation equally. The cost of maintaining the argument of perigee is close to 11 m/s per year. Maneuvers to correct for Earth oblateness will likely have to be made on a daily basis. Other perturbation effects also disrupt the circular and projected circular formations, but the cost of correcting these effects is much smaller compared to the J_2 effects.

Unlike the formation keeping, the station keeping cost for the classes of orbits discussed here is relatively small. Only atmospheric drag decay of the semimajor axis is a major concern. Velocity impulse to correct for this effect is on the order of 1.5 m/s per year using high-drag conditions.

Because maneuver requirements can vary within a formation (particularly for the circular and projected circular formation designs), some indirect formation keeping issues will arise. Once the masses of the satellites in the formations vary, differential drag effects will be much larger. These effects, however, should still be small in comparison to the J_2 effects.

Other major issues that impact the frequency and cost of formation keeping maneuvers are attitude control, the precision of the propulsion system, and navigation accuracy. The formation keeping maneuvers discussed require thrusting in the along-track, cross-track, and radial directions. The satellite dynamics are very sensitive to accelerations in the along-track directions. The largest maneuvers are required in the cross-track and radial directions. If the satellite pointing has substantial errors when cross-track or radial maneuvers are performed, some unwanted acceleration may be applied in the along-track direction with significant consequences. Also, the propulsion system must be capable of delivering precise and accurate thrusts because small errors map directly into errors in the desired orbital elements. These errors will undoubtedly drive the frequency and cost of formation keeping higher than what is presented here.

Orbit determination knowledge is another factor that will influence formation control. The propagations show that centimeter-level differences in semimajor axis cause significant along-track error growth over time. The ability to determine the orbits to this level of precision is vital for precise and efficient formation control.

Note that some mean element capability was required to perform this analysis. The formation flying designs are performed using two-body dynamics. When propagating these formation flying designs in the presence of perturbations, care must be taken to ensure that the mean-to-osculating conversion is done correctly. If elements from the two-body dynamics design are assumed to be osculating, unnecessary errors will be introduced into the propagations. For example, if the semimajor axes found after conversion from Hill's equations[8] are assumed to be osculating in the presence of J_2, the mean semimajor axes will be different, resulting in formation dispersion caused by different orbital periods. The dispersion may be confused with a real perturbation effect when it is actually an error in application. In this analysis, the DSST AOG was used to propagate the mean element equations directly.

Acknowledgments

The authors would like to thank Rich Cobb, Mike Stallard, and Maurice Martin of the U.S. Air Force Research Laboratory (AFRL) TechSat 21 Office for supporting this effort. The authors also thank Jesse Leitner for his support of the AFRL Spaceflight Dynamics and Control group. The authors are also indebted to Terry Alfriend for his insightful suggestions in the preparation of this paper. Additional thanks go to Megan Bir, Kim Luu, Scott Carter, David Spencer, and Jeff Beck of the AFRL Space Vehicles Directorate, as well as Henry Warchall (University of North Texas) for their help.

References

[1] Folta, D. C., Newman, L. K., and Gardner, T., "Foundations of Formation Flying for Mission to Planet Earth and New Millenium," *Proceedings of the AIAA/AAS Astrodynamics Conference*, AIAA, Reston, VA, 1996, pp. 656–666.

[2] Bauer, F., Bristow, J., Folta, D., Hartman, K., and Quinn, D., "Satellite Formation Flying Using an Innovative Autonomous Control System AUTOCON Environment," AIAA Paper 97-3821, Aug. 1997.

[3] Roux, A., "Cluster Regroups for Relaunch," *Aerospace America*, Vol. 36, No. 8, 1998, pp. 48–51.

[4] How, J. P., Twiggs, R., Weidow, D., Hartman, K., and Bauer, F., "Orion: A Low-Cost Demonstration of Formation Flying in Space Using GPS," AIAA Paper 98-4398, Aug. 1998.

[5] Folkner, W. M., Hechler, F., Sweetser, T. H., Vincent, M. A., and Bender, P. L., "LISA Orbit Selection and Stability," *Classical and Quantum Gravity*, Vol. 14, June 1997, pp. 1405–1410.

[6] Das, A., Cobb, R., and Stallard, M., "TechSat 21: A Revolutionary Concept in Distributed Space Based Sensing," AIAA Paper 98-5255, Oct. 1998.

[7] Martin, M., and Stallard, M., "Distributed Satellite Missions and Technologies—The TechSat 21 Program," AIAA Paper 99-4479, Sept. 1999.

[8] Hill, G. W., "Researches in the Lunar Theory," *American Journal of*

Mathematics, Vol. 1, No. 1, 1878, pp. 5–26.

[9]Sedwick, R. J., Kong, E. M. C., and Miller, D. W., "Expoiting Orbital Dynamics and Micropropulsion for Aperture Synthesis Using Distributed Satellite Systems: Applications to TechSat 21," AIAA Paper 98-5289, Oct. 1998.

[10]Vallado, D. A., *Fundamentals of Astrodynamics and Applications*, edited by W. J. Larson, Space Technology Series, McGraw–Hill, New York, 1997, pp. 264–268, 343–368, 567–602, 763–773.

[11]Lawden, D. F., *Optimal Trajectories for Space Navigation*, Butterworths, London, 1963, pp. 77–86.

[12]Inalhan, G., and How, J. P., "Relative Dynamics and Control of Spacecraft Formations in Eccentric Orbits," AIAA Paper 2000-4443, Aug. 2000.

[13]Spencer, D., "The Effects of Eccentricity on the Evolution of an Orbiting Debris Cloud," American Astronautical Society, AAS Paper 87-473, Aug. 1987.

[14]McClain, W., "A Recursively Formulated First-Order Semianalytic Artificial Satellite Theory Based on the Generalized Method of Averaging," Computer Sciences Corp., TR NAS 5-2400, June 1978.

[15]Danielson, D. A., "Semianalytic Satellite Theory," Naval Postgraduate School, TR NPS-MA-95-002, Monterey, CA, 1994.

[16]Feiger, M. E., "An Evaluation of Semianalytic Satellite Theory Against Long Arcs of Real Data for Highly Eccentric Orbits," M.S. Thesis, Massachussets Inst. of Technology, Cambridge, MA, Jan. 1995.

[17]Sabol, C., Cefola, P., and Metzinger, R., "Application of Sun-Synchronous, Critically Inclined Orbits to Global Personal Communications Systems," American Astronautical Society, AAS Paper 95-222, Feb. 1995.

[18]Fonte, D. J., "PC Based Orbit Determination," AIAA Paper 94-3776, Aug. 1994.

[19]Schatten, K. J., Scherrer, P. H., Svalgaard, L., and Wilcox, J. M., "Using Dynamo Theory to Predict the Sunspot Number During Solar Cycle 21," *Geophysical Research Letters*, Vol. 5, No. 5, 1978, pp. 411–414.

[20]Sofia, S., Fox, P., and Schatten, K., "Forecast Update for Activity Cycle 23 from a Dynamo-Based Method," *Geophysical Research Letters*, Vol. 25, No. 22, 1998, pp. 4149–4152.

[21]Alfriend, K. T., Schaub, H., and Gim, D.-W., "Gravitational Perturbations, Nonlinearity and Circular Orbit Assumption Effects on Formation Flyinc Control Strategies," American Astronautical Society, AAS Paper 00-012, Jan. 2000.

[22]Battin, R. H., *An Introduction to the Mathematics and Methods of Astrodynamics*, AIAA Education Series, AIAA, Washington, DC, 1987, pp. 484–490.

C. A. Kluever
Associate Editor